Additive Manufacturing 36 (2020) 101577

Contents lists available at ScienceDirect

Additive Manufacturing

journal homepage: www.elsevier.com/locate/addma

Heat treatment possibilities for an in situ βTi-TiC composite made by laser powder bed fusion

Sasan Dadbakhsh [a,b,*], Raya Mertens [a], Gang Ji [c], Bey Vrancken [d,e], Kim Vanmeensel [d], Haiyang Fan [a], Ahmed Addad [c], Jean-Pierre Kruth [a]

[a] PMA/MaPS, Department of Mechanical Engineering, KU Leuven & Member of Flanders Make, Leuven, 3001, Belgium
[b] Department of Production Engineering, KTH Royal Institute of Technology, Stockholm SE-10044, Sweden
[c] Univ. Lille, CNRS, INRAE, Centrale Lille, UMR 8207 - UMET - Unité Matériaux et Transformations, F-59000, Lille, France
[d] Department of Materials Engineering, KU Leuven, Leuven, 3001, Belgium
[e] Materials Science Division, Lawrence Livermore National Laboratory, Livermore, CA, 94550, USA

ARTICLE INFO

Keywords:
Heat-treatment
Titanium alloy
In situ metal matrix composites
Additive manufacturing
Laser powder processing

ABSTRACT

After laser powder bed fusion (LPBF) of an ultra-strong in situ TiC whisker reinforced β-Ti composite, this paper investigates the evolution of microstructure and mechanical properties in response to heat treatment at different temperatures. Using in depth nano-SEM and TEM analyses, it is shown that ageing at 400 °C rounds the whiskers, annihilates the strain fields and grows Mo segregated nano-cells, but without improving the ductility. In contrast, ageing at 600 °C enables the transformation of metastable β to a lamellar β + α, leading to a dual phase matrix embedding TiC particles. This is in such a manner that extra ageing at 600 °C coalesces the nano-lamellar α + β microstructure to form a coarser micro-lamellar α + β matrix. This microstructure achieves 66 % of the compressive deformation of Cp-Ti, and over 1400 MPa compressive strength after 1 h of ageing at 600 °C. Despite this success under compression, hard and stiff TiC particles may still cause large spherical fractured voids, severely limiting the plastic deformation under tension.

1. Introduction

The goal of using metal matrix composites (MMCs) is to combine the toughness from metals and stiffness from ceramics and intermetallics. This goal, however, is not easy to achieve due to several difficulties such as weak interfacial reinforcement-matrix bonding, imperfect morphology of reinforcements, cracks at the interfaces, inhomogeneous reinforcement distributions, residual stresses, and/or dislocations induced by thermal mismatches between composing phases [1]. To overcome these difficulties, in situ techniques in which the reinforcements are created via an in situ chemical reaction, are becoming more popular [2–4]). These can be particularly applied within laser powder bed fusion (LPBF) (also known as selective laser melting - SLM) [4], which is the main additive manufacturing (AM) technique for manufacturing metals.

LPBF is in fact a powder-based technique allowing for a controlled layer-wise fabrication of metal components from any designated powder mixture. This enables the fabrication of complicated geometrical shapes from in situ reactive metal materials, yielding the generation of fine and hard reinforcements during LPBF. Examples given in the literature mainly include LPBF of in situ fabricated Al MMCs starting from Al-Fe_2O_3, Al-SiC and Al-ZnO powder mixtures [5–8], as well as-LPBF of Ti MMCs from Ti + Si_3N_4, Ti + TiB_2 and Ti-Mo-Mo_2C powder mixtures [9–14].

The current work focuses on the latest in situ Ti composite system, i.e., Ti-Mo_2C. For this system, very recent and promising developments have been made by the authors [14,15]. Within these works, a strong and hard Ti alloy composite without potentially cytotoxic elements such as Al and V was developed using the LPBF process. Within LPBF of Ti+10.5 wt%Mo_2C powder mixture [15], it was observed that Mo_2C progressively decomposed to Mo and carbon in the Ti melt. The former stabilised the β-Ti phase (instead of martensitic α-phase), while the latter formed in situ TiC whiskers with high aspect ratios (50−200 nm wide and up to several micrometres long). The generated hard TiC whiskers established an excellent interfacial bonding with β-Ti matrix. As a result, the developed in situ TiC whisker reinforced β-Ti had a high hardness of 513 HV and the compressive strength of about 1642 MPa. In fact, without the use of Al and V as strengthening but cytotoxic elements, the

* Corresponding author.
E-mail address: sdad@kth.se (S. Dadbakhsh).

https://doi.org/10.1016/j.addma.2020.101577
Received 29 June 2020; Received in revised form 19 August 2020; Accepted 28 August 2020
Available online 9 September 2020

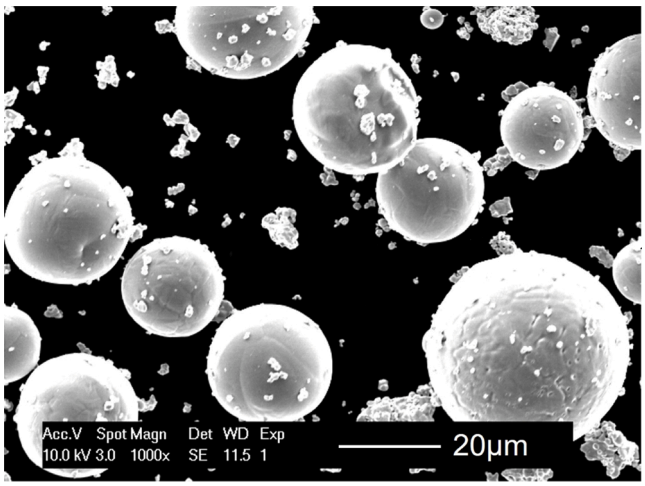

Fig. 1. Powder mixture of Ti/10.5 wt%Mo_2C. Large spherical Cp-Ti particles are decorated with fine Mo_2C agglomerated particles.

hardness and strength of pure titanium was increased using biocompatible Mo [16] and in situ TiC whisker reinforcements (which can even stimulate bioactivity [17,18]). However, on the downside, no plastic deformation was observed in the as built product. To improve the extreme brittleness, Vrancken et al. [14] used a powder system with a lower amount of Mo_2C (3.5 wt%) and instead an additional amount of Mo (6.5 wt%), to achieve a similar β stabilizing effect. Lowering the amount of Mo_2C to about one-third in the initial powder allowed some plastic deformation under compression, but the real change in ductility and strength was obtainable via heating the material to higher temperature.

Despite such promising research, the heat treatment possibilities and the corresponding phenomena to change the microstructure and control the mechanical properties are not yet understood. These are complicated phenomena since it involves formation and transformation of various Ti solid phases such as beta (β), omega (ω), and alpha (α) [19–22] in the presence of secondary TiC particles with a complex whisker morphology [14,15]. Understanding these phenomena is vital to manipulate the ductility, especially since high contents of secondary reinforcements has an extreme effect on brittleness. Accordingly, the present work has been dedicated to investigate the possible heat treatments at different temperatures and the corresponding driving mechanisms influencing the ductility in brittle LPBF made in situ Ti-TiC.

To this end, this work carries out ageing heat treatment at different temperatures of 400 °C when β can transform to ω and 600 °C when β transforms to α according to the literature [22]. The effects of these heat

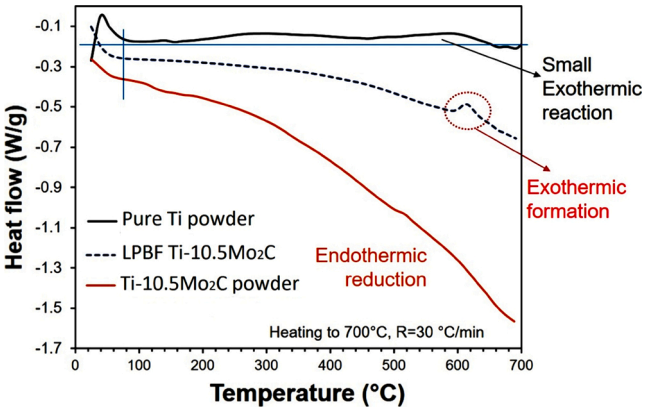

Fig. 2. DSC curves of pure Ti powder, Ti/10 wt%Mo_2C powder, and LPBF parts made from Ti/10 wt%Mo_2C.

treatments on the hardness are studied and the microstructural features are analysed using XRD, nanoSEM and TEM. After recognising the transformation phenomena during these treatments, mechanical tests are performed both in compression and tension in order to assess the strength and ductility of the composite material.

2. Materials and methods

2.1. Materials and LPBF

Gas atomised Cp-Ti powder (grade 1), obtained from LPW Ltd (UK) with a particle size ranging from 15 µm to 45 µm, was mixed with 10.5 wt% molybdenum carbide powder (Mo_2C, Changsha Langfeng, China) with an average particle size of ~3.5 µm. This amount of Mo_2C would theoretically generate 9.88 wt% Mo and 0.62 wt% C after decomposition. This powder system was dry mechanically mixed on a Turbula for 8 h. Despite the agglomeration of Mo_2C particles which is common for fine powders, this resulted in a sufficiently homogeneous mixture (Fig. 1) in which agglomerated Mo_2C particles fill the space between spherical Ti powder particles. The remaining Mo_2C particles after Turbula mixing reduced the flowability of the powder without impeding LPBF processing.

A commercial 3DS ProX 320 LPBF machine with a 400 W fibre laser and a beam diameter of about 60 µm was used to manufacture samples under a protective argon atmosphere (oxygen was well below 100 PPM). A laser power of 300 W, scanning speed of 1000 mm/s, layer thickness of 30 µm and hatch spacing of 70 µm were applied as optimum parameters to reach dense (> 99.0 % density) and crack free parts [15]. This was done using a bi-directional scanning strategy with 90° rotation between the layers.

2.2. Post heat treatment and characterisation

The transformation behaviour of both powders and LPBF parts were characterised by METTLER TOLEDO differential scanning calorimetry (DSC) with a heating rate of 30 °C min^{-1} from room temperature to 700 °C. To reassure of the measurements for calibration purposes, the onset for the melting of indium was checked to have a lag below 0.2 °C at different heating rates.

The LPBF parts were heat treated at 400 °C and 600 °C in a furnace and cooled in air. The temperature was double-checked using an extra thermocouple close to the specimens. To have an early understanding of the effect of post heat-treatment, Vickers micro hardness tests were performed using a Future Tech FV-700 hardness tester with an indentation load of 1 kg. All cross-sections were cut, polished and prepared along the LPBF building direction.

Phase identification was done by X-ray diffraction (XRD, Bruker D2 Seifert 3003 TT X-ray diffractometer) in a Theta/2Theta set-up with Cu-$K_{\alpha 1}$ radiation operated at 40 kV and 40 mA. To analyse the microstructure, a FEI-Nova Nanosem 450 equipped with EBSD detector was used. Transmission electron microscopy (TEM) was performed using two instruments. The first one was a FEI Tecnai TEM, operated at 200 kV and equipped with a Nanomegas ASTAR system and a Bruker XFlash 6T160 EDX unit. The second one was a FEI Titan Themis 300, operated at 200 kV, and equipped with a probe aberration corrector and a highly efficient (4 quadrant) EDX system. TEM disk samples were prepared using mechanical polishing and final ion thinning using a GATAN precision ion polishing system. The phase sizes were measured based on the scale of the micrographs. The sizes were presented from at least 8 readings.

Compression tests were carried out using a 250 kN INSTRON universal testing machine. This was performed with a crosshead speed of 0.3 mm/min within hardened tool steel compressive plates at room temperature. The compression was parallel to the LPBF building direction. The compression samples were cuboids with 6 mm × 6 mm and about 10 mm height. Zinc stearate was used as lubricant at the compression plates. It should be noted that the deformation of the

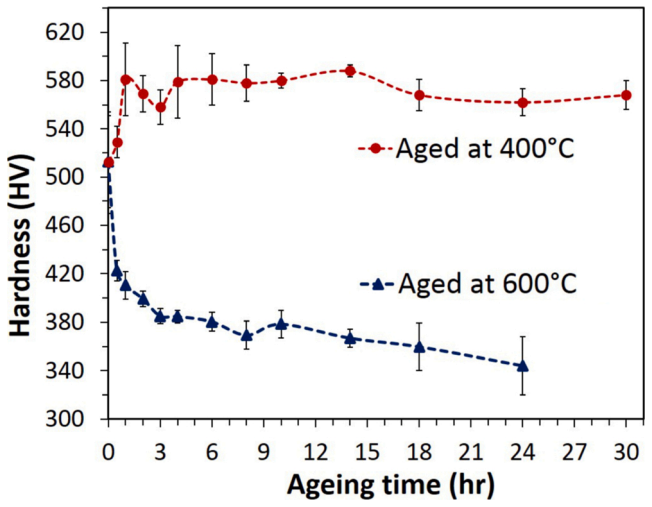

Fig. 3. Hardness evolution of LPBF made Ti/Mo_2C parts due to ageing at 400 °C and 600 °C.

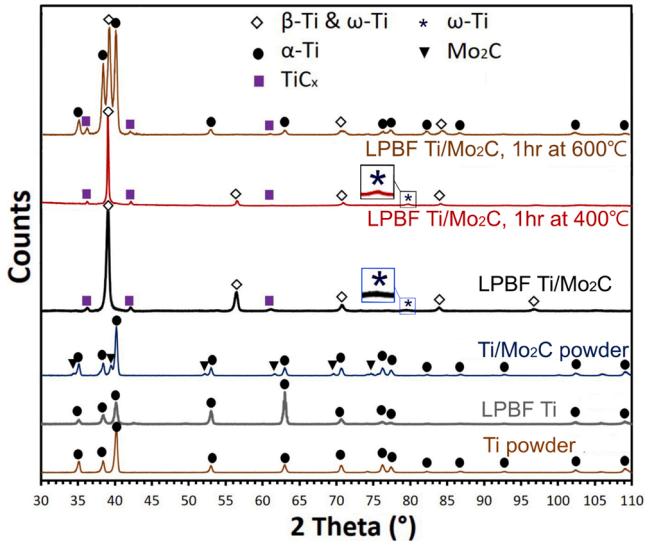

Fig. 4. XRD spectra of Ti and Ti/Mo_2C powder and parts including after ageing at 400 °C and 600 °C. Note that β-Ti and ω-Ti are detected at the same peaks despite they are different Ti allotropes.

compression steel plates (present at the top and bottom of the samples) during compression could also contribute to the measured strains, although this could not be filtered out. Therefore, the strains especially at elastic regions were not accurate and were only used for comparison purposes. In addition to compression, tensile tests were carried out using an Instron machine with 30 kN load cell and extensometer on subsize specimens according to ASTM E8.

3. Results

3.1. DSC

Fig. 2 shows the DSC curves of Ti and Ti/Mo_2C powders as well as of a LPBF part from Ti/Mo_2C powder. As seen, the DSC curve of Ti powder appears mostly horizontal despite some small exothermic reaction that is most likely due to the presence of small amount of air beside argon, allowing formation of oxides and nitrides. In comparison, the DSC curve of Ti/Mo_2C drastically drops indicating endothermic changes in the material until 700 °C. For the LPBF parts, DSC curves are something in between with an addition of an exothermic peak slightly above 600 °C.

3.2. Hardness

Fig. 3 shows the hardness evolution of the LPBF parts after ageing at 400 °C and 600 °C for different ageing times. As seen, the hardness after ageing at 400 °C increases at first and after a primary increase it may decrease. This is completely in contrast to the early sharp drop followed by slow reduction of hardness after ageing at 600 °C.

3.3. XRD

Ti can appear with different allotropes such as α, ω, and β. The α-Ti phase is hexagonal closed-packed where each basal plane is a hexagonal layer with a stacking pattern of ABAB. β-Ti is a high temperature body-centred cubic (BCC) which can transform to ω only when cooled under pressure, due to the collapse of BCC planes in the [111] direction. ω-Ti is a metastable phase with a hexagonal structure similar to α-Ti, but it has a low c/a ratio in comparison to α-Ti. This means the distance between the basal planes is short and the spacing in the hexagonal lattice is very wide in ω-Ti [23].

Fig. 4 shows the XRD spectra of the pure Ti powder and LPBF part from Ti/Mo_2C as well as the LPBF parts from Ti/Mo_2C after ageing at 400 °C and 600 °C. As seen, the recognised phases from the XRD spectrum change to β-Ti (cubic BCC) instead of α-Ti (hexagonal) after LPBF beside a minority of TiC secondary phase. However, this is not yet a stable structure since the ageing alters the XRD peaks. This is in such a manner that α-Ti evidently increases after ageing at 600 °C even only for 1 h. In contrast to ageing at 600 °C, ageing at 400 °C for 1 h does not cause any clear change in the XRD spectrum of the LPBF part. It should be noted that ω-Ti may also form or exist, but it cannot be individually identified since its peaks coincide with β-Ti peaks. This is except for only one weak peak at about 2 theta = 79.7°, as boldly demonstrated using the magnified insets for the spectra of as-LPBF and 1 h ageing at 400 °C.

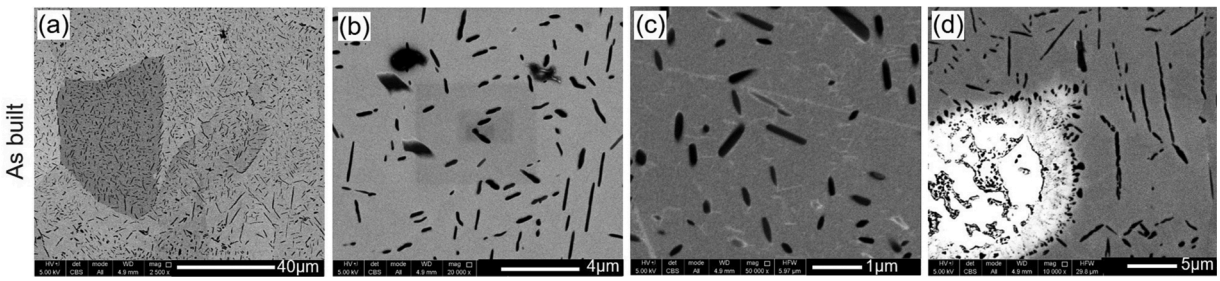

Fig. 5. Typical microstructure of as-LPBF composite parts containing a relatively homogenous distribution of whisker shape titanium carbides in a granular Ti matrix (a-c), while a very minority of unreacted Mo_2C-Mo-C may exist (d).

3.4. NanoSEM

Fig. 5 shows the typical microstructure of the LPBF part from Ti/10.5 wt%Mo_2C. As observed, addition of Mo_2C completely changes the microstructural characteristics, leading to a very homogeneous distribution of secondary whisker-shaped particles in a Ti matrix. Within the Ti matrix, in contrast to pure Ti LPBF material, no acicular and lath-like α′ (martensitic α) phases are observable [24,25]. The secondary whisker-shaped particles are very fine and exist with a width of typically less than 150 nm and lengths that can reach up to several micrometres (Fig. 5b-c). Occasionally, very small amount of unreacted Mo_2C-Mo-C may remain after LPBF (Fig. 5d). This occurs rarely, when the Mo_2C particles were excessively agglomerated in the powder mixture (as some seen in Fig. 1), requiring more laser energy or laser exposure duration to achieve full dissociation.

Fig. 6 shows the microstructure of LPBF parts after ageing at 400 °C. As observed after 1 h, the aspect ratio of the whisker shaped TiC secondary whiskers is reduced (Fig. 6b). At the same time, stretching lines as a sign of strained fields appear inside the matrix (Fig. 6b-c). Looking deeper into the matrix, very fine nano-precipitates with a size of typically 15−40 nm also exist in the matrix. More ageing up to 30 h at 400 °C further evolves the microstructure by rounding and spheroidising TiC whiskers (Fig. 6f-g) as well as growing the nano precipitates to typically 20−50 nm. After different durations, the main difference is the annihilation of the stretching lines (strained fields) due to further ageing at this temperature (compare Fig. 6c and g).

In comparison to ageing at 400 °C, ageing at 600 °C severely alters the microstructure as seen in Fig. 7. In fact, ageing at 600 °C generates

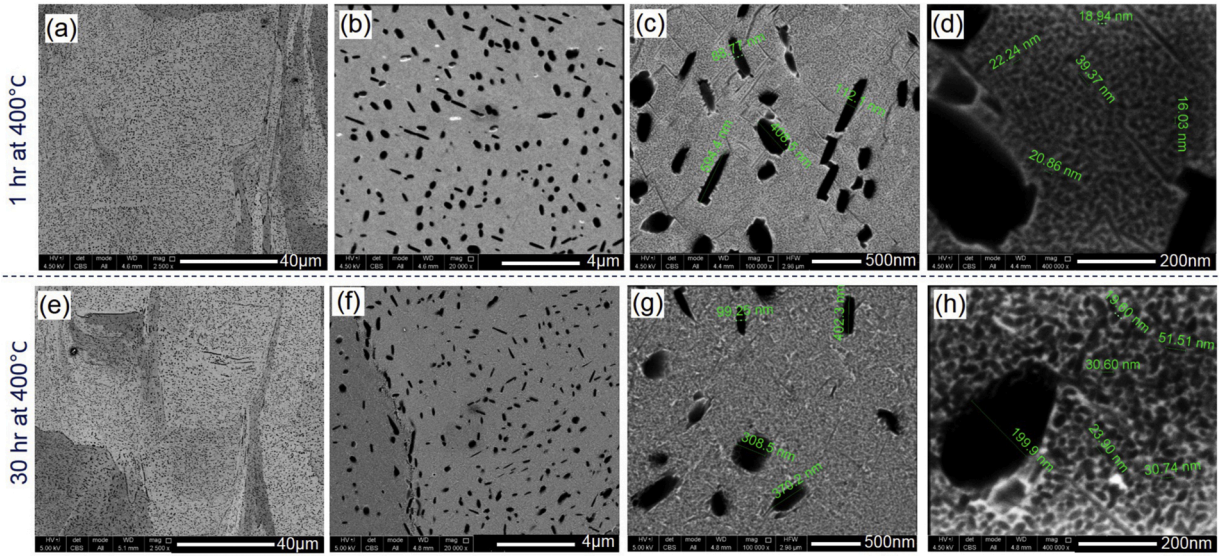

Fig. 6. Microstructure of LPBF Ti/Mo_2C parts, aged for (a-d) 1 h and (e-h) 30 h at 400 °C.

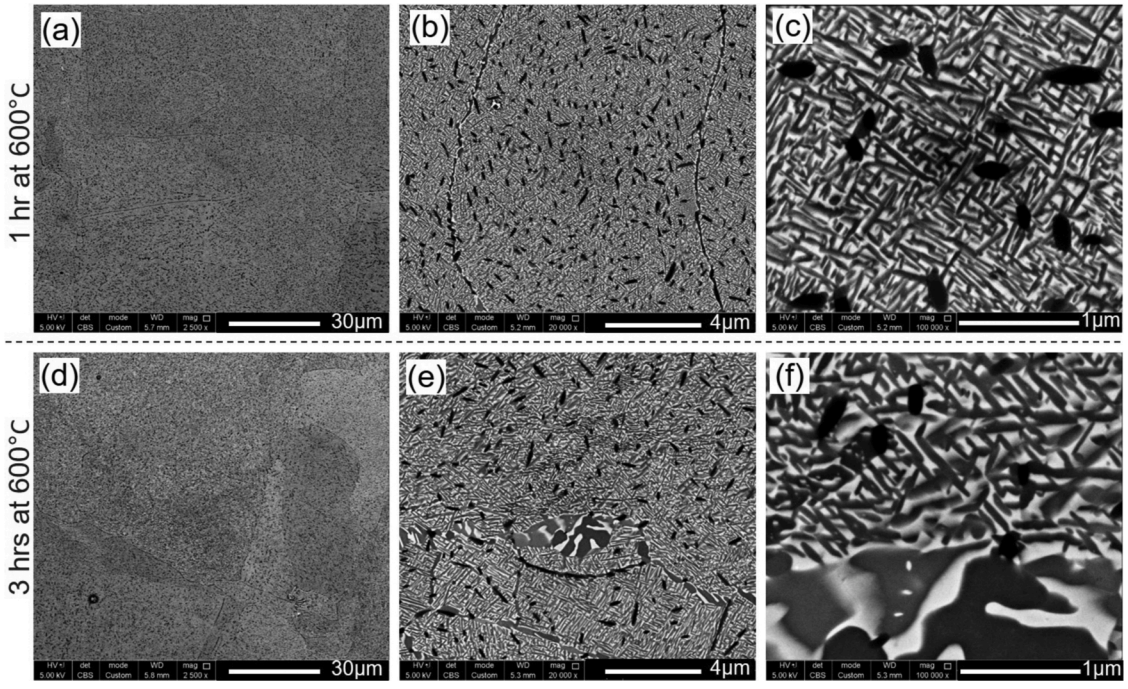

Fig. 7. Microstructures of LPBF Ti/Mo_2C parts, aged for (a-c) 1 h and (d-f) 3 h at 600 °C.

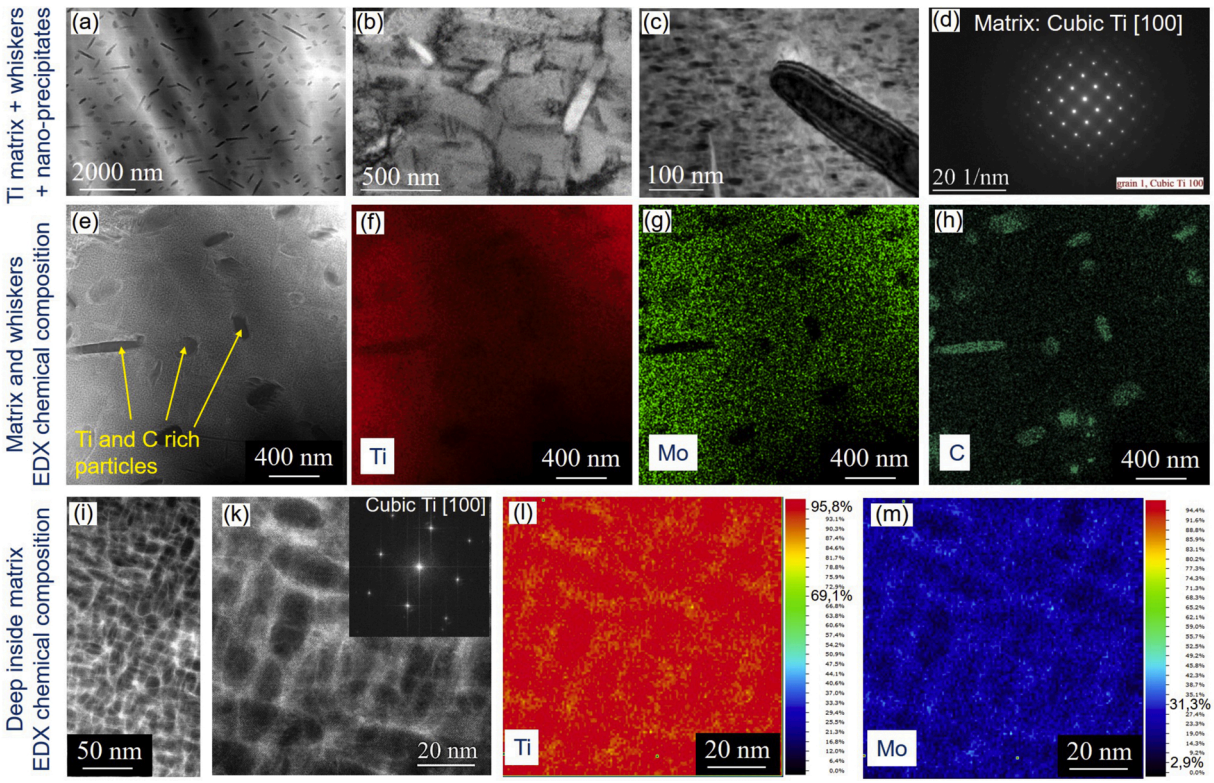

Fig. 8. TEM investigations showing the microstructural details of as-LPBF Ti/Mo_2C parts.

acicular and lath-like α leading to vertically formed dark laths in the white β-Ti matrix in addition to slightly rounded TiC whiskers (Fig. 7b-c). Further ageing at 600 °C may allow the phases to coalesce, shown as a local globular appearance of dual phases after 3 h ageing (Fig. 7e-f).

3.5. TEM

TEM investigations on the as-LPBF parts allow a more detailed understanding of the nanoscale features existing in the matrix, as shown in Fig. 8. In fact, by looking deep into the whisker reinforced matrix, some signs of strain can be seen around the TiC whiskers (Fig. 8b) in the cubic BCC Ti matrix (Fig. 8d). Also, the matrix may contain very fine nano precipitates beside TiC whiskers (Fig. 8c). EDX on the overall microstructure shows that Ti (Fig. 8f) and Mo (Fig. 8g) compositions are relatively homogenous in the microstructure, while carbon mainly exists on the whisker particles beside Ti (Fig. 8h) where no Mo is present (Fig. 8g). Accordingly, the secondary whisker shaped particles are mainly from Ti and C (Fig. 8e) which corresponds to titanium carbide. This is in agreement with the previous work that had mainly shown these secondary particles as TiC whiskers [15]. This partly owed to the rapid release of carbon followed by rapid solidification and partly to the role of Mo in Ti which reduces the carbon solubility in β-Ti and promotes formation of secondary particles as TiC whiskers [15,26]. Focussing further on the matrix, nano-segregation can be observed in composition generating the nano precipitates in previous pictures. However, here these nano-precipitates look more like nano-cells which contain less Mo and more Ti within the interior in comparison with the boundaries (Fig. 8i-m). This structure also corresponds to cubic Ti.

In comparison, after ageing at 400 °C, TEM shows strain fields in perpendicular patterns, as seen in Fig. 9a (as a sign of strain field in agreement with Fig. 6c). At this stage, nano-cells tend to cover the matrix (Fig. 9e). After 6 h of ageing at 400 °C, nano-cells grow larger while the strain zones disappear (Fig. 9c-d). This is while the matrix remains cubic Ti (Fig. 9e).

In comparison with ageing at 400 °C, ageing at 600 °C transforms the microstructure to a dual phase matrix composed of HCP Ti (Fig. 10c) and cubic Ti (Fig. 10d) embedding a minority of TiC whiskers (Fig. 10a-b). The cubic Ti looks to be connected mainly as one grain over the shown scale in Fig. 10d, while embedding numerous HCP Ti nanosize grains (Fig. 10c). As seen, these phases are hardly recognisable since phases are well adhered and no cracking can be observed at the interfaces.

3.6. Compressive and tensile properties

Fig. 11 shows the compressive properties of the in situ assisted LPBF made composites before and after ageing. As seen from Fig. 11a, as-LPBF parts are extremely brittle without any sign of plasticity even under compressive forces despite their very high compressive strength 1642 ± 77 MPa. Ageing at 400 °C for 6 and 24 h did not also change this extreme brittleness, as the parts broke after elastic regions only at a bit of lower strengths. In contrast, as shown in Fig. 11b, ageing at 600 °C for 1–4 h drastically increases the ductility and the plastic deformation. For example, 66 % of ductility of Cp-Ti can be reached only after 1 h of ageing at 600 °C. This is of course in the expense of a successive decrease in the strength to about 1420 MPa after 1 h aging and to about 1320 MPa after 4 h of ageing. However, the material is still significantly stronger than pure titanium after LPBF.

Fig. 12 shows the tensile properties of the developed in situ reinforced Ti composite without ageing and after 1 h of ageing at 600 °C, compared to pure Ti. As demonstrated, the tensile strength of the composite will be 1261 ± 38 MPa, being more than twice the UTS of LPBF made pure titanium (around 550 MPa). The composite stiffness (~107.4 ± 2.0 GPa) is comparable to the stiffness of pure titanium (~106.5 ± 2.5 GPa) despite the presence of softer β-Ti in the aged composite. However, the ductility under tension is still very low (barely reaching 3–4 %) in comparison to the high elongation of pure titanium

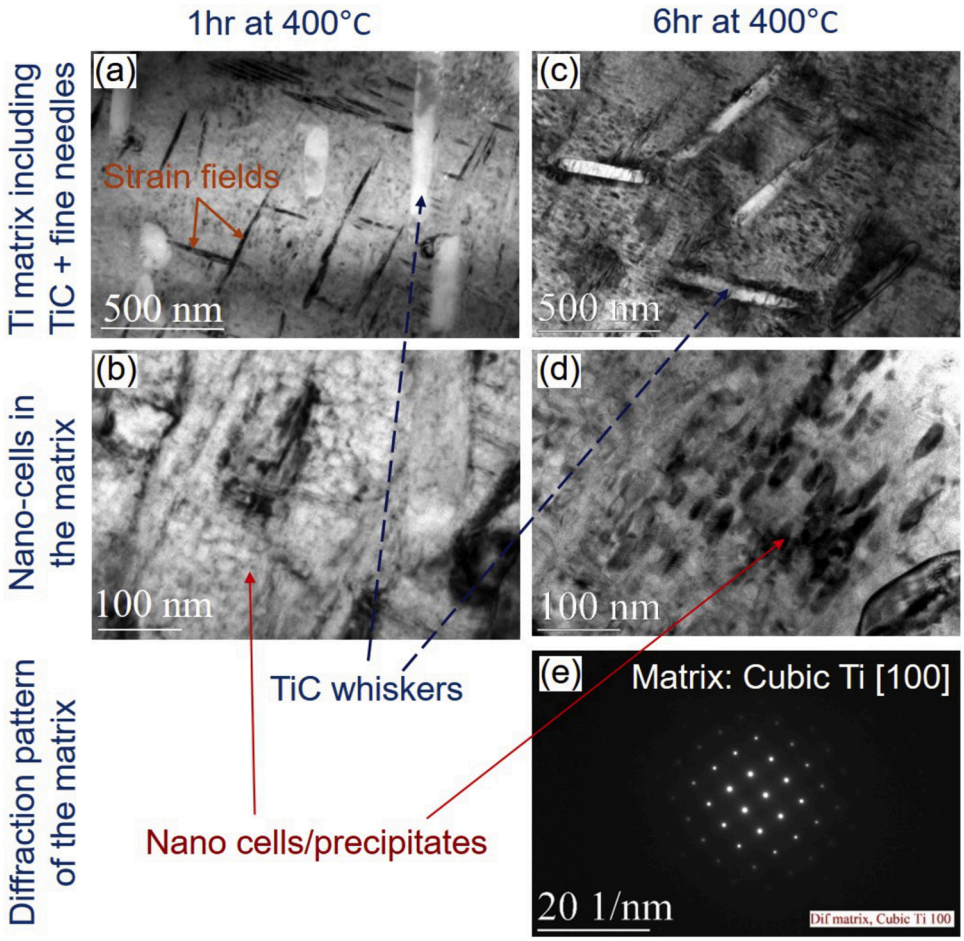

Fig. 9. TEM images showing the detailed microstructural evolution due to (a-b) 1 h and (c-e) 6 h ageing at 400 °C.

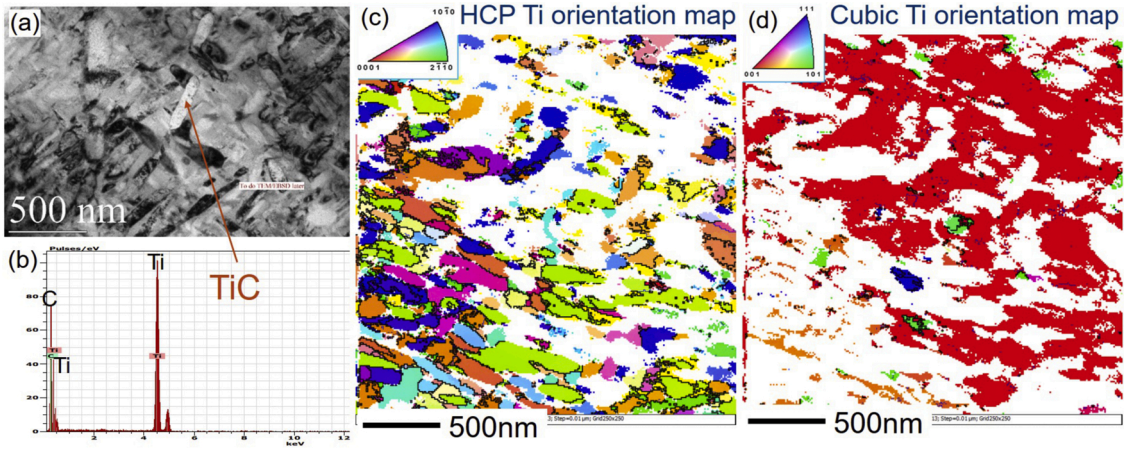

Fig. 10. TEM investigations showing the microstructural details after 1 h of ageing at 600 °C.

that can reach 17–18 %.

4. Discussion

4.1. Ageing phenomena at 400 °C

The extreme condition of LPBF (high temperature and rapid solidification/cooling) in conjunction with in situ transformations in the current case of Ti/Mo_2C have led to a metastable TiC reinforced β-Ti matrix, seeking to become stable if allowed (see the XRD spectrum in Fig. 4). This is the driving force for transformation after receiving adequate activation energy at different ageing temperatures (such as at 400 °C and 600 °C).

Exposing the material to 400 °C retains the overall microstructure, but at the same time causes some changes (compare Fig. 5 and Fig. 8 to Fig. 6 and Fig. 9). For example, the whisker shape TiC particles become more rounded, i.e., they clearly become thicker and shorter after 30 h of ageing (see Fig. 6f-h). This can be attributed to the tendency of the TiC as

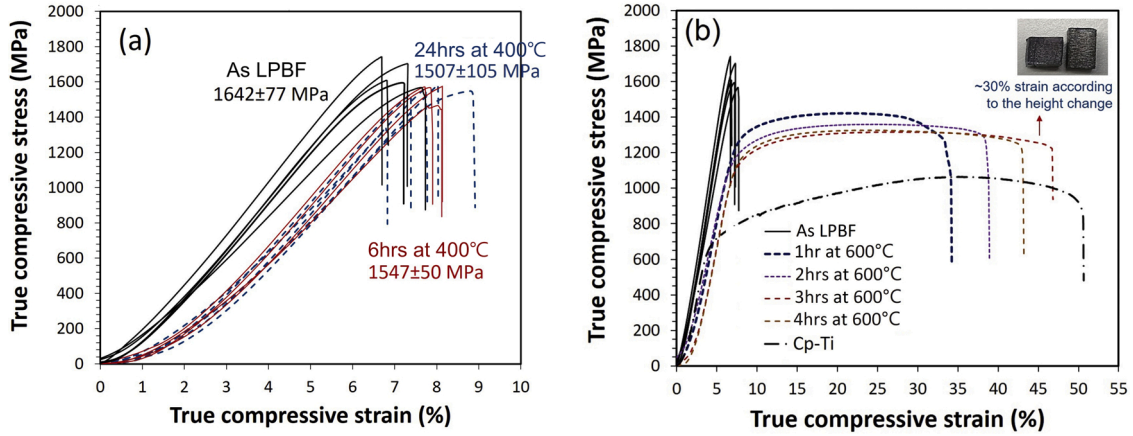

Fig. 11. True compressive stress-strain curves before and after ageing (a) at 400 °C for 6 h and 24 h and (b) at 600 °C for 1-4 h in comparison with pure titanium.

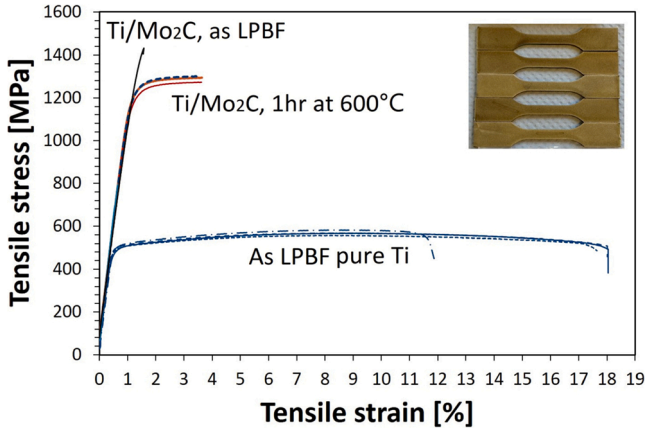

Fig. 12. Tensile properties before and after ageing at 600 °C for 1 h in comparison with pure titanium.

a cubic material to grow to octahedron and consequently spherical shapes [27,28] instead of elongated whiskers which had been imposed by directional TiC crystal growth during LPBF [15]. This indicates a high mobility of carbon in the TiC and/or Ti matrix at this temperature due to its small atomic size.

The morphological change of TiC whiskers (from whisker towards a spherical shape) generates strain fields in the cubic crystal structure of β-Ti matrix. If transformation of β→ω also occurs (as a possibility, although this was not detected in TEM studies), it could also cause volume change and shear and hence elastic strain [22,29–31]. These appear as strain fields in perpendicular orientations (Fig. 9a) according to the perpendicular slipping planes of a BCC structure. This is beside the fact that the formation of TiC whiskers had also imposed residual stresses during solidification and cooling down, as shown as strain fields in the as-LPBF composite material (Fig. 8b). Nevertheless, after only 6 h of ageing at 400 °C, these strain fields have diminished in the microstructure. This indicates that recovery mechanisms to annihilate the dislocations had become influential for ageing times longer than 1 h at 400 °C for this particular metastable β-Ti matrix.

In addition to morphological changes of TiC as well as formation and annihilation of the strain fields at 400 °C, the growth of nano-cells/precipitates (Fig. 8c) covering the Ti matrix is another phenomenon. These originate from nano-segregation of Mo from cubic Ti crystals (Fig. 8i-k). The growth of these nano-cells (for example see Fig. 6d and h after 1 h and 30 h of ageing at 400 °C) facilitates the transformation of cubic β-Ti to α-Ti within the nano-cells. Although this cannot be clearly confirmed in the TEM results of this work, the middle product of this transformation could be perhaps ω-Ti to allow an easy and low energy transformation from β-Ti at temperatures below 500 °C [22,32] in the form of nano precipitates [33,34]. This is in agreement with the XRD results that show β-Ti and the possibility of having ω-Ti after 1 h ageing at 400 °C (see Fig. 4). Nevertheless, it can be concluded that Mo has a limited/slow mobility in Ti matrix at 400 °C due to its very large atomic size especially in comparison with C atoms. This hinders the drastic transformations driven by the metastable status of the matrix at 400 °C.

4.2. Ageing phenomena at 600 °C

Within the starting powder, there is a tendency for Mo_2C to decompose in the neighbourhood of Ti to generate more stable TiC.

Table 1
Sizes of the β-Ti, titanium carbide and α-Ti in as-LPBF and after 1 h ageing at 400 °C and 600 °C within LPBF building direction. After the average values, the values shown in the bracket demonstrate the size range of the phase.

Condition	β-Ti		Titanium carbide			α-Ti	
	Width (μm)	Depth* (μm)	Width (nm)	Length (nm)	Aspect ratio (length/width)	Width (nm)	Length (nm)
As-LPBF	83 ± 18 (50–120)	NA** (40–340)	190 ± 62 (120–360)	NA** (370–6800)	9 ± 6 (3–22)	—	—
1 h aged at 400 °C	62 ± 32 (10–100)	79 ± 52 (20–210)	191 ± 84 (110–350)	NA** (300–2000)	NA** (1–13)	—	—
1 h aged at 600 °C	23 ± 13 (7–45)	22 ± 9 (12–35)	124 ± 34 (70–180)	358 ± 105 (230–560)	3.1 ± 1.3 (1.8–5.7)	39 ± 10 (25–55)	375 ± 140 (170–600)

* Note: since the measurements has been performed along the building direction, the depth of β-grains demonstrate the height of the β-grains in the building direction.

** Note: To keep the presented data scientifically meaningful, NO average (NA) has been shown where the standard deviation was too high over 80 % of the average value.

However, for decomposition of Mo_2C, first some energy is required. This leads to the sharp drop in the DSC curve of Ti + Mo_2C powder, as an endothermic heat to decompose Mo_2C powder. After LPBF, the endothermic reduction can still appear, even though the drop is less intensive (Fig. 2). This reduction could be partly because of the possibility of the remaining Mo_2C particles (Fig. 5d) and partly due to the diffusion of Mo and C atoms in the matrix. At about 600 °C, the diffusion of Mo finally enables the β→α transformation which appears as an exothermic peak in the DSC curve of the LPBF Ti/Mo_2C part (Fig. 2). The diffusion occurs since 10 wt% Mo is not adequate to fully stabilise β-Ti [29], leading to a β + α matrix after 1 h of ageing at 600 °C, as seen in Fig. 10. It should be mentioned that with the diffusion of Mo, C can remain and act as α-Ti stabiliser [35]. C can also diffuse in the matrix and within the TiC structure, enabling morphological changes of the TiC whiskers.

The aforementioned phenomena mainly occurs due to the high mobility of Mo in the Ti matrix at the higher temperature of 600 °C, imposing many fundamental microstructural changes as shown in Fig. 7 and Fig. 10. This is in such a manner that single phase and smooth β-Ti matrix in the as-LPBF parts (Fig. 5) turn into a nano-lamellar structure from β-Ti (white colour in BSE) and α-Ti (darker colour in BSE) phases embedding black TiC particles only after 1 h of ageing at 600 °C (Fig. 7c and Fig. 10). This is also seen in the XRD spectra as generation and growth of α peaks next to β peaks (e.g., see 1 h at 600 °C spectrum in Fig. 4). Further ageing at 600 °C may coalesce this nano-lamellar α + β microstructure, as the starting point for formation of a micro-lamellar α + β matrix (Fig. 7e-f).

4.3. Size evolution of the main phases due to ageing

For the microstructures shown in Fig. 5 to Fig. 10, Table 1 summarises the size evolution of the main phases after ageing. As seen, β grains become finer, even when the part is aged at 400 °C but particularly when it is aged at 600 °C. This seems to be due to tendency of the crystal structure to increase the angles of β grain boundaries by relieving the internal stresses and the β→α transformation. At the same time, TiC carbides fragment and/or dissolve in the matrix and become smaller. This is particularly evident when the ageing temperature is higher at 600 °C. Since the transformation of β-Ti to α-Ti is fully active at 600 °C, this can also be attributed to the higher solubility of carbon in α-Ti compared to β-Ti (being 0.48 wt% for α-Ti vs. only 0.15 wt% for β-Ti for pure titanium at 920 °C [35]), driving the C dissolution. Simultaneously, the aspect ratio of the carbides reduces in order to reach a lower energy. Lastly, only at 600 °C, nano size α-Ti rapidly forms in the larger β-Ti grains. This reinforces the softer β-Ti grains by acicular and lath-like α-Ti metal.

It is worth mentioning that with ageing above 600 °C and below 800 °C (approximately when the β is not yet fully stable), the natural phenomenon is the accelerated microstructural coarsening of the newly formed α-Ti. This means that at higher temperatures the newly formed α-Ti grains grow faster. This is equal to longer ageing times at lower temperatures (which would successively reduce the strength and increase the ductility), as seen in Fig. 7f. Therefore, to avoid excessive microstructural coarsening, ageing at a lower temperature of 600 °C has been carried out here. This has allowed a finer microstructural control while the β→α transformation has been fully active.

4.4. Correlation of mechanical properties with post treatments

The compression yield stress in LPBF Cp-Ti with a martensitic α-phase, as the basis of this material without any alloying element, is about 670 ± 10 MPa. The yield strength increases drastically around 1000 MPa after adding 10.5 wt% Mo_2C to Ti powder in this work. This drastic strengthening (along with the extreme brittleness) could originate from a multitude of influential factors. They include i) the metastable β-Ti structure with nano segregation of dissolved Mo, ii) fine size, high fraction, high aspect morphology and relatively homogeneous distribution of in situ made titanium carbides as the secondary particles, iii) the dissolved carbon in metastable β-Ti and iv) the residual stresses hidden in the material structure after LPBF. Among these, the metastable β-Ti structure saturated by Mo seems to be the top influencer. This is since only after transformation of the metastable β-Ti to stable α + β Ti structure, a drastic change in the strength and ductility occurs (e.g., see the significant loss of strength and drastic increase of ductility via ageing at 600 °C in Fig. 11b against the slight changes in the strength and ductility via ageing at 400 °C in Fig. 11a). After this, the second influential factor could be the high fraction of high aspect ratio TiC whiskers with excellent bonding all over the matrix. These whiskers allow no plasticity without their own deformation or displacement. Since TiC is a hard ceramic, it remains strong until the loads under compressive deformation increases to a value much greater than the matrix. At this stage, the β-Ti matrix catastrophically fails from the regions around the actual TiC whiskers [15]. The third factor, i.e., the dissolved carbon in Ti as an interstitial element, could have been another reason to increase the strength of solid solution [35], although the abundant amount of TiC particles seem to have consumed all the carbon. This is in agreement with the decreased solubility of carbon in highly alloyed beta-titanium alloys [36]. The last factor, i.e., the residual stresses, can also lock the nano-cells in the matrix. This could be indeed relieved after ageing at higher temperatures.

Focusing on the mechanical properties via ageing at 400 °C, the hardness (Fig. 3) first increases until 1 h due to generation of large strain fields with the initiation of the changes in the matrix (Fig. 6c and Fig. 9a). After that, the hardness slightly decreases with the annihilation of strain fields in the matrix (Fig. 6g and Fig. 9c). This is followed by creation of a smooth secondary peak in hardness (Fig. 3). This could be perhaps due to precipitation of intermediate ω-Ti, as commonly observed at 400 °C from a metastable β-Ti [22]. It should be noted that ω-Ti was not confirmed by TEM inspections (possibly due to its very small size and the local changes in the material), although some very weak ω-Ti signature appeared in XRD spectrum after ageing at 400 °C as seen in Fig. 4. Nevertheless, ω-Ti has been reported to be brittle but with a high hardness and stiffness [29,33]. In addition, the nano segregation of Mo elements as nano-cells (Fig. 8i-m) can hamper the deformation. Moreover, the presence of TiC particles can also reduce the ductility [37]. These lead to high brittleness of the material even under compressive loadings (Fig. 11a). This is despite the fact that ageing at 400 °C slightly reduces the compression strength (perhaps due to lower aspect ratio of the carbides) and is seemingly successful in recovering the matrix from residual stresses and strain fields.

In contrast to ageing at 400 °C, ageing at 600 °C significantly increases the ductility in the expense of lowering the strength and hardness (Fig. 11b and Fig. 3) by transforming the microstructure. In fact, ageing at 600 °C provides adequate mobility for Mo to diffuse and form Mo-rich regions, stabilising the β-grains. Simultaneously, this creates Mo-poor regions behind, causing the transformation of β-Ti to α-Ti. These transformations form acicular nano α-Ti (see the nano sizes in Table 1) within softer and more stable β-crystals (see Fig. 7 and Fig. 10). This microstructure does not any longer contain any segregated nano-cell or any residual strain fields that could potentially hamper the plastic deformation. In addition, titanium carbides are smaller with a lower aspect ratio (see Table 1) facilitating the plastic flow of the material. As a result, the strength drops while ductility increases. It should be noted that although the β-Ti seem to have a lower grain size after ageing at 600 °C (Table 1), this effect is masked against other factors due to the active transformation of β→α which rapidly decreases the β volume fraction.

Despite an evident increase in ductility under compressive loading via ageing at 600 °C (Fig. 11b), the tensile elongation cannot yet match the pure titanium (Fig. 12). This can be attributed to the role of hard and stiff TiC whiskers with an extremely good interface with the matrix. In fact, under tension, the stresses may concentrate and raise around the largest TiC whiskers. With the increase of tensile stress above 1200 MPa,

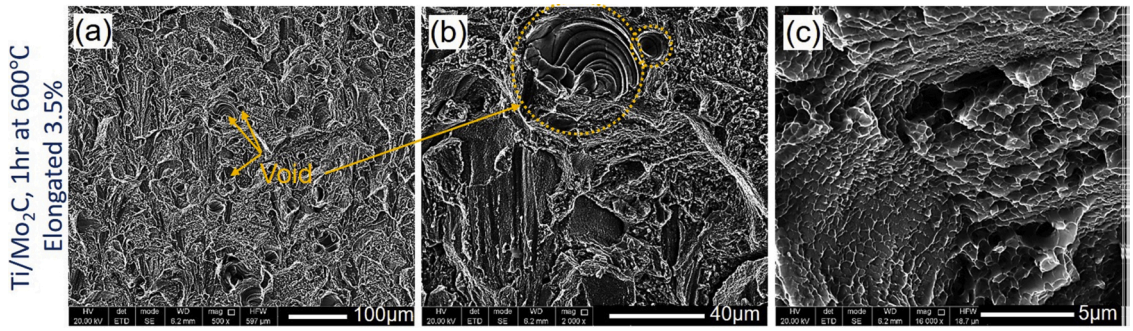

Fig. 13. Fractured surfaces of Ti reinforced composite after ageing at 600 °C for 1 h, showing (a-b) fractured voids typically with some sudden deformation signature between 10 to 40 μm in the matrix, which (c) appear to be deformed as submicron cells.

the stress around the largest TiC particles accumulates to a larger value which can be easily adequate to cause a shear between the stressed zone and the matrix. As a result, the stressed zones are pulled apart from the matrix, leaving fractured voids with some sudden deformation signature around 10−40 μm (Fig. 13a-b). These voids can join under tension and cause a rapid failure, despite the matrix is seemingly ductile with deformed cells in submicron ranges (Fig. 13c). This material however shows high ductility under compression (Fig. 11b) where, even in the case of stress-induced-voids, the voids are closed by compressive forces until shear collapses the material.

It is worth mentioning that although the tensile elongation of the current composite (which is made without strengthening by cytotoxic elements such as Al and V) is still rather limited, most biomedical load bearing implants (for bone replacement and dental applications) function mostly under compressive loading. The presented ductility under compressive loads is sufficiently high (close to Cp-Ti, see Fig. 11b). Moreover, higher ductility under tension should be still achievable, but it requires even finer secondary reinforcements. This is ideally down to less than 10 nm (as common in precipitation hardening of alloys). This might be done for example by replacing a part of the Mo_2C with pure Mo and/or a better powder preparation practice (e.g., use of ball milling to embed single Mo_2C particles instead of agglomerated bunches) to generate TiC particles even below 10−20 nm.

5. Conclusions

This work investigated the evolution of an in situ TiC reinforced β-Ti composite in response to ageing heat treatment at different temperatures of 400 °C and 600 °C. The aim was to investigate the influence of various heat treatments on the microstructure and the material ductility. Accordingly, it was found that:

- The microstructure of the in situ LPBF composite, composed of TiC whiskers in cubic β-Ti matrix, was not stable. As a result, the microstructure and the consequent properties largely evolved upon heating to higher temperatures.

- Carbon atoms with their small sizes were mobile in the TiC and/or Ti matrix at 400 °C. Therefore, the whisker shape of TiC particles became more rounded via ageing at this temperature. The shape change of TiC whiskers at 400 °C imposed some strain, forming perpendicular strain fields in the cubic crystal structure of β-Ti matrix. However, prolonged ageing annihilated these strain fields.

- Nano-segregation of Mo in the β-Ti matrix appeared as nano-cells. These nano-cells could slowly grow via ageing at 400 °C. However, this by itself did not improve the matrix ductility.

- Around 600 °C, the diffusion of Mo was sufficient to allow the metastable β→α transformation to occur. As a result, only after 1 h of ageing at 600 °C, single phase β-Ti matrix turned into a nano-lamellar structure from β-Ti and α-Ti phases embedding black TiC particles. Further ageing at 600 °C may coalesce this nano-lamellar α + β microstructure to become a coarser micro-lamellar α + β matrix. Such microstructure contained smaller and lower aspect ratio TiC whiskers which was also free from any segregated nano-cells or any residual strain fields that could potentially hamper the plastic deformation.

- The metastable β to lamellar β + α transformation due to ageing at 600 °C significantly increased the ductility in the expense of lowering the strength and hardness. This, only after 1 h of ageing at 600 °C, resulted in a strength of 1420 MPa and a ductility level of 66 % of Cp-Ti under compressive loads.

- Via ageing at 600 °C, despite the ductile nature of the β + α matrix under compressive loading and high UTS of ~1260 MPa under tension, the tensile elongation could not match the pure titanium. This was attributed to the role of hard and stiff TiC particles causing fractured pores typically between 10−40 μm under tension.

Author contributions

In this work, S.D. was the main author, researcher and experimental designer; R.M. was the researcher, experimentalist and analyser; G.J. carried out and analysed the TEM results; B.V. provided ideas and interpretations. K.V. was the co-supervisor; H.F. helped with the microstructural experiments. A.A. carried out the TEM tests using FEI Titan; JP.K. was the main supervisor.

Data availability

Microstructural data generated or analysed during this study are included in this published article. Extra and raw data are available upon request from the corresponding author.

Declaration of Competing Interest

The authors report no declarations of interest.

Acknowledgments

This work was supported by the Flanders Innovation & Entrepreneurship agency (Agentschap Innoveren en Ondernemen (VLAIO)) in the framework of the Strategic Basic Research (SBO) project “MultiMet” - Grant No. 150010. Gang JI thanks “Bourses de mobilité transfrontalière” from I-site ULNE foundation. The microscopy facilities in Lille (France) are supported by the Conseil Régional du Nord-Pas de Calais, and the European Regional Development Fund (ERDF).

References

[1] S. Suresh, A. Mortensen, A. Needleman, Preface, in: S. Suresh, A. Mortensen, A. Needleman (Eds.), Fundamentals of Metal-Matrix Composites, Butterworth-Heinemann, Boston, 1993, pp. vii–viii, https://doi.org/10.1016/B978-0-08-052371-2.50003-1.

[2] I.A. Ibrahim, F.A. Mohamed, E.J. Lavernia, Particulate reinforced metal matrix composites - a review, J. Mater. Sci. 26 (1991) 1137–1156, https://doi.org/10.1007/BF00544448.
[3] S.C. Tjong, Z.Y. Ma, Microstructural and mechanical characteristics of in situ metal matrix composites, Mater. Sci. Eng. R Rep. 29 (2000) 49–113, https://doi.org/10.1016/S0927-796X(00)00024-3.
[4] S. Dadbakhsh, R. Mertens, L. Hao, J. Van Humbeeck, J.-P. Kruth, Selective laser melting to manufacture "In situ" metal matrix composites: a review, Adv. Eng. Mater. 21 (2019) 1801244, https://doi.org/10.1002/adem.201801244.
[5] S. Dadbakhsh, L. Hao, P.G.E. Jerrard, D.Z. Zhang, Experimental investigation on selective laser melting behaviour and processing windows of in situ reacted Al/Fe2O3 powder mixture, Powder Technol. 231 (2012) 112–121, https://doi.org/10.1016/j.powtec.2012.07.061.
[6] S. Dadbakhsh, L. Hao, Effect of Al alloys on selective laser melting behaviour and microstructure of in situ formed particle reinforced composites, J. Alloys Compd. 541 (2012) 328–334, https://doi.org/10.1016/j.jallcom.2012.06.097.
[7] F. Chang, D. Gu, D. Dai, P. Yuan, Selective laser melting of in-situ Al4SiC4+SiC hybrid reinforced Al matrix composites: influence of starting SiC particle size, Surf. Coat. Technol. 272 (2015) 15–24, https://doi.org/10.1016/j.surfcoat.2015.04.029.
[8] S. Dadbakhsh, R. Mertens, K. Vanmeensel, J. Vleugels, J.V. Humbeeck, J.-P. Kruth, In situ alloying and reinforcing of Al6061 during selective laser melting, Procedia CIRP 74 (2018) 39–43, https://doi.org/10.1016/j.procir.2018.08.009.
[9] D. Gu, C. Hong, G. Meng, Densification, microstructure, and wear property of in situ titanium nitride-reinforced titanium silicide matrix composites prepared by a novel selective laser melting process, Metall. Mater. Trans. A 43 (2012) 697–708, https://doi.org/10.1007/s11661-011-0876-8.
[10] D. Gu, Y. Shen, Z. Lu, Preparation of TiN–Ti5Si3 in-situ composites by selective laser melting, Mater. Lett. 63 (2009) 1577–1579, https://doi.org/10.1016/j.matlet.2009.04.010.
[11] H. Attar, M. Bönisch, M. Calin, L.C. Zhang, K. Zhuravleva, A. Funk, S. Scudino, C. Yang, J. Eckert, Comparative study of microstructures and mechanical properties of in situ Ti–TiB composites produced by selective laser melting, powder metallurgy, and casting technologies, J. Mater. Res. 29 (2014) 1941–1950, https://doi.org/10.1557/jmr.2014.122.
[12] H. Attar, M. Bönisch, M. Calin, L.-C. Zhang, S. Scudino, J. Eckert, Selective laser melting of in situ titanium–titanium boride composites: processing, microstructure and mechanical properties, Acta Mater. 76 (2014) 13–22, https://doi.org/10.1016/j.actamat.2014.05.022.
[13] H. Attar, K.G. Prashanth, L.-C. Zhang, M. Calin, I.V. Okulov, S. Scudino, C. Yang, J. Eckert, Effect of powder particle shape on the properties of in situ Ti–TiB composite materials produced by selective laser melting, J. Mater. Sci. Technol. 31 (2015) 1001–1005, https://doi.org/10.1016/j.jmst.2015.08.007.
[14] B. Vrancken, S. Dadbakhsh, R. Mertens, K. Vanmeensel, J. Vleugels, S. Yang, J.-P. Kruth, Selective Laser Melting process optimization of Ti–Mo–TiC metal matrix composites, CIRP Ann. (2019), https://doi.org/10.1016/j.cirp.2019.04.120.
[15] S. Dadbakhsh, R. Mertens, K. Vanmeensel, G. Ji, J.-P. Kruth, In situ transformations during SLM of an ultra-strong TiC reinforced Ti composite, Sci. Rep. 10 (2020) 10523, https://doi.org/10.1038/s41598-020-67434-3.
[16] A.M. Ribeiro, T.H.S. Flores-Sahagun, R.C. Paredes, A perspective on molybdenum biocompatibility and antimicrobial activity for applications in implants, J. Mater. Sci. 51 (2016) 2806–2816, https://doi.org/10.1007/s10853-015-9664-y.
[17] M. Brama, N. Rhodes, J. Hunt, A. Ricci, R. Teghil, S. Migliaccio, C.D. Rocca, S. Leccisotti, A. Lioi, M. Scandurra, G. De Maria, D. Ferro, F. Pu, G. Panzini, L. Politi, R. Scandurra, Effect of titanium carbide coating on the osseointegration response in vitro and in vivo, Biomaterials 28 (2007) 595–608, https://doi.org/10.1016/j.biomaterials.2006.08.018.
[18] G. Longo, C.A. Ioannidu, A. Scotto d'Abusco, F. Superti, C. Misiano, R. Zanoni, L. Politi, L. Mazzola, F. Iosi, F. Mura, R. Scandurra, Improving osteoblast response in vitro by a nanostructured thin film with titanium carbide and titanium oxides clustered around graphitic carbon, PLoS One 11 (2016) e0152566, https://doi.org/10.1371/journal.pone.0152566.
[19] P.C. Collins, R. Banerjee, S. Banerjee, H.L. Fraser, Laser deposition of compositionally graded titanium–vanadium and titanium–molybdenum alloys, Mater. Sci. Eng. A 352 (2003) 118–128, https://doi.org/10.1016/S0921-5093(02)00909-7.
[20] A. Almeida, D. Gupta, C. Loable, R. Vilar, Laser-assisted synthesis of Ti–Mo alloys for biomedical applications, Mater. Sci. Eng. C 32 (2012) 1190–1195, https://doi.org/10.1016/j.msec.2012.03.007.
[21] B. Vrancken, L. Thijs, J.P. Kruth, J. Van Humbeeck, Microstructure and mechanical properties of a novel β titanium metallic composite by selective laser melting, Acta Mater. 68 (2014) 150–158, https://doi.org/10.1016/j.actamat.2014.01.018.
[22] F. Langmayr, P. Fratzl, G. Vogl, W. Miekeley, Crossover from ω-phase to α-phase precipitation in bcc Ti-Mo, Phys. Rev. B 49 (1994) 11759–11766, https://doi.org/10.1103/PhysRevB.49.11759.
[23] D. Rhea Trinkle Iii, A Theoretical Study of the HCP to Omega Martensitic Phase Transition in Titanium, The Ohio State University, 2003. Doctor of Philosophy Thesis.
[24] H. Attar, S. Ehtemam-Haghighi, D. Kent, X. Wu, M.S. Dargusch, Comparative study of commercially pure titanium produced by laser engineered net shaping, selective laser melting and casting processes, Mater. Sci. Eng. A 705 (2017) 385–393, https://doi.org/10.1016/j.msea.2017.08.103.
[25] B. Wysocki, P. Maj, A. Krawczyńska, K. Rożniatowski, J. Zdunek, K. J. Kurzydłowski, W. Święszkowski, Microstructure and mechanical properties investigation of CP titanium processed by selective laser melting (SLM), J. Mater. Process. Technol. 241 (2017) 13–23, https://doi.org/10.1016/j.jmatprotec.2016.10.022.
[26] Z.Q. Chen, Y.G. Li, M.H. Loretto, Role of alloying elements in microstructures of beta titanium alloys with carbon additions, Mater. Sci. Technol. 19 (2003) 1391–1398, https://doi.org/10.1179/026708303225005999.
[27] J. Nie, X. Liu, X. Ma, Influence of trace boron on the morphology of titanium carbide in an Al–Ti–C–B master alloy, J. Alloys Compd. 491 (2010) 113–117, https://doi.org/10.1016/j.jallcom.2009.10.148.
[28] D. Gu, Y. Shen, G. Meng, Growth morphologies and mechanisms of TiC grains during selective laser melting of Ti–Al–C composite powder, Mater. Lett. 63 (2009) 2536–2538, https://doi.org/10.1016/j.matlet.2009.08.043.
[29] P. Cao, F. Tian, Y. Wang, Effect of Mo on the phase stability and elastic mechanical properties of Ti–Mo random alloys from ab initio calculations, J. Phys. Condens. Matter 29 (2017) 435703, https://doi.org/10.1088/1361-648x/aa87d3.
[30] M.J. Lai, C.C. Tasan, J. Zhang, B. Grabowski, L.F. Huang, D. Raabe, Origin of shear induced β to ω transition in Ti–Nb-based alloys, Acta Mater. 92 (2015) 55–63, https://doi.org/10.1016/j.actamat.2015.03.040.
[31] F. Sun, D. Laillé, T. Gloriant, Thermal analysis of the ω nanophase transformation from the metastable β Ti–12Mo alloy, J. Therm. Anal. Calorim. 101 (2010) 81–88, https://doi.org/10.1007/s10973-010-0713-0.
[32] J. Ruzic, S. Emura, X. Ji, I. Watanabe, Mo segregation and distribution in Ti–Mo alloy investigated using nanoindentation, Mater. Sci. Eng. A 718 (2018) 48–55, https://doi.org/10.1016/j.msea.2018.01.098.
[33] W.F. Ho, Effect of omega phase on mechanical properties of Ti-Mo alloys for biomedical applications, J. Med. Biol. Eng. 28 (2008) 47–51.
[34] M.C. Jon, H. Fujimura, R.J. De Angelis, Omega-phase formation in Beta III titanium alloy, Metallography 5 (1972) 139–150, https://doi.org/10.1016/0026-0800(72)90051-1.
[35] O.P. Solonina, N.M. Ulyakova, Effect of carbon on the mechanical properties and structure of titanium alloys, Met. Sci. Heat Treat. 16 (1974) 310–312, https://doi.org/10.1007/BF00679223.
[36] L.A. Petrova, E.V. Dyomina, V.S. Khlomov, The effect of carbon on the behavior of the Beta-titanium alloys, in: J.C. Williams, A.F. Belov (Eds.), Titanium and Titanium Alloys: Scientific and Technological Aspects, Vol. 3, Springer US, Boston, MA, 1982, pp. 2217–2227, https://doi.org/10.1007/978-1-4757-1758-7_57.
[37] R. Banoth, R. Sarkar, A. Bhattacharjee, T.K. Nandy, G.V.S. Nageswara Rao, Effect of boron and carbon addition on microstructure and mechanical properties of metastable beta titanium alloys, Mater. Des. 67 (2015) 50–63, https://doi.org/10.1016/j.matdes.2014.11.004.